Hofstadter butterflies in a modulated magnetic field: Superconducting wire network with magnetic decoration

Yasuhiro Iye,* Eiichi Kuramochi, Masahiro Hara, Akira Endo, and Shingo Katsumoto
Institute for Solid State Physics, University of Tokyo, 5-1-5 Kashiwanoha, Kashiwa, Chiba 227-8581, Japan
(Received 1 April 2004; published 29 October 2004)

Hofstadter butterfly spectra of tight-binding electron systems under spacially modulated magnetic fields are calculated. The dependence of the spectrum on the symmetry and strength of the spatially varying magnetic field is elucidated. The Little-Parks oscillation of the superconducting network under a spatially modulated magnetic field produced by decoration with mesoscopic magnetic structure exhibits behavior reproducing the edge of the corresponding Hofstadter spectra.

DOI: 10.1103/PhysRevB.70.144524 PACS number(s): 74.78.−w, 74.81.Fa, 75.75.+a, 73.21.−b

I. INTRODUCTION

The exquisite structure of the energy diagram of a tight-binding electron system on a two-dimensional (2D) square lattice subjected to a uniform perpendicular magnetic field was first elucidated by the work of Hofstadter[1] and Wannier.[2] The spectrum consists of q subbands, when the flux α (in the units of the flux quantum $\phi_0=h/e$) threading through each plaquette is a rational number p/q. The spectra of this type, known as the Hofstadter butterfly, have since been calculated for a variety of lattices,[3–5] and they have been discussed in various contexts of condensed-matter physics including the quantum Hall effect[6,7] and the so-called flux phase in the t-J model.[8,9]

Observation of the butterfly spectra in real systems is a formidable task. For the ordinary crystalline lattices, the required magnetic field exceeds 1000 T, which is beyond the reach of the present technology. It is therefore natural to turn to the artificial periodic structures, such as lateral superlattices based on semiconductor two-dimensional electron systems. Recent work by Albrecht *et al.*[10] on magnetotransport in an antidot lattice seems to capture a certain characteristic of the Hofstadter spectrum.

Superconducting networks comprise another category of systems intimately related to the Hofstadter spectrum. As demonstrated by Pannetier *et al.*,[11] the change in the transition temperature of a superconducting wire network with the frustration parameter α reproduces the fine structure of the upper edge of the Hofstadter butterfly spectrum. This correspondence arises from the fact that the linearized Ginzburg-Landau equation for a superconductor near its transition has the same form as the Schrödinger equation for the electron system.[12,13] Thus, with the advantage of macroscopic coherence, superconducting networks provide a convenient experimental model of the Hofstadter butterfly, although admittedly they can only probe the edge of the spectrum. This line of study was subsequently extended to networks of various lattice symmetries, including triangular, honeycomb, Kagomé,[14] $\mathcal{T}_3$,[15] disordered,[16] quasiperiodic,[17] and fractal[18] lattices.

To the best of our knowledge, all of these previous studies basically employed a uniform external magnetic field. It would be interesting to extend the study to more general cases of spatially varying magnetic field. This is the subject of the present study. More specifically, we have calculated the Hofstadter spectrum for a square lattice under spacially varying magnetic fields. We have also conducted experiments using a superconductor/ferromagnet (S/F) hybrid system consisting of a superconducting wire network and an array of mesoscopic ferromagnets. An early version of our study using an S/F hybrid system study has been published.[19,20] An S/F hybrid system of a different type from the present one was studied by Nozaki *et al.*[21] The Hofstadter spectrum for a $\mathcal{T}_3$ lattice under a modulated magnetic field is theoretically studied by Oh.[22]

The remainder of this paper is organized as follows. Calculations of the Hofstadter spectra for a square network under various patterns of a spatially varying magnetic field are presented in the next section. Experiments using a superconductor/ferromagnet hybrid system are described in Sec. III, and discussed in comparison with the calculated spectra. Finally, Sec. IV gives a summary of the present work and some remarks.

II. CALCULATION OF THE HOFSTADTER SPECTRA

A. The original Hofstadter problem

The Hofstadter problem in its original form, i.e., the tight-binding electron spectrum on a 2D square lattice with lattice constant a under a uniform magnetic field H, is obtained by solving the following Schrödinger equation:

$$\varepsilon\psi_{n,m} = t\psi_{n-1,m} + t\psi_{n+1,m} + te^{-2\pi in\alpha}\psi_{n,m-1} + te^{2\pi in\alpha}\psi_{n,m+1}, \tag{1}$$

where $\psi_{n,m}$ represents the wave function at the lattice site (n,m), t is the nearest-neighbor transfer-matrix element, and $\alpha \equiv \phi/\phi_0 = eHa^2/h$ is an avarage magnetic flux threading a unit square. The parameter α is often called a frustration parameter. The above equation can be reduced by putting

$$\psi_{n,m} = e^{ik_x na}e^{ik_y ma}\varphi_n \tag{2}$$

to the following one-dimensional Harper equation:

 ©2004 The American Physical Society

$$\varepsilon\varphi_n = te^{-ik_x a}\varphi_{n-1} + te^{ik_x a}\varphi_{n+1} + 2t\cos(k_y a - 2\pi n\alpha)\varphi_n. \tag{3}$$

When α is a rational number p/q, p and q being mutually prime, the size of the magnetic unit cell becomes (qa,a), namely, $\psi(x+qa,y)=\psi(x,y)$ and $\psi(x,y+a)=\psi(x,y)$. Figure 1 shows the tight-binding square lattice with the choice of gauge appropriate to $\alpha=p/q$. The energy eigenvalues are obtained by diagonalizing the following matrix:

$$\begin{pmatrix} 2t\cos(k_y a-2\pi\alpha) & te^{ik_x a} & 0 & \cdots & 0 & e^{-ik_x a} \\ te^{-ik_x a} & 2t\cos(k_y a-4\pi\alpha) & te^{ik_x a} & 0 & \cdots & 0 \\ 0 & \ddots & \ddots & \ddots & & \vdots \\ \vdots & & 0 & \ddots & \ddots & 0 \\ 0 & \cdots & 0 & te^{-ik_x a} & 2t\cos[k_y a-2(q-1)\pi\alpha] & te^{ik_x a} \\ te^{ik_x a} & 0 & \cdots & 0 & te^{-ik_x a} & 2t\cos(k_y a-2q\pi\alpha) \end{pmatrix}. \tag{4}$$

The result is the well-known butterfly spectrum, shown in the topmost panel of Fig. 3.

B. Checkerboard magnetic field

We consider a spatially varying magnetic field which consists of a uniform component and a component varying in a checkerboard pattern, as shown in Fig. 2. Here, α denotes the flux per plaquette of the uniform component of the magnetic field, and β denotes the flux per plaquette which alternates in sign in the checkerboard pattern. The assignment of the Peierls phase factor for this flux pattern is shown in the figure. For $\alpha=p/q$, the system is invariant under translation $(2qa,0)$ or (a,a). The relevant Schrödinger equation reads

$$\varepsilon\psi_{n,m} = t\psi_{n-1,m} + t\psi_{n+1,m} + te^{-2\pi i[(n-m+1)\alpha}\psi_{n,m-1} + te^{2\pi i(n-m)\alpha}e^{2\pi i\beta}\psi_{n,m+1}\ (n-m\ \text{odd}), \tag{5}$$

$$\varepsilon\psi_{n,m} = t\psi_{n-1,m} + t\psi_{n+1,m} + te^{-2\pi i(n-m+1)\alpha}e^{2\pi i\beta}\psi_{n,m-1} + te^{2\pi i(n-m)\alpha}\psi_{n,m+1}\ (n-m\ \text{even}).$$

Spectra obtained by diagonalization of the corresponding $2q\times 2q$ matrix are shown in Fig. 3. The spectra are symmetric with respect to transformations, $\beta\rightarrow 1\pm\beta$, so that calculation over the range $\beta=0-\frac{1}{2}$ suffices. Five panels in Fig. 3 correspond to $\beta=0$, $\frac{1}{8}$, $\frac{1}{4}$, $\frac{3}{8}$, and $\frac{1}{2}$, respectively. The topmost panel $(\beta=0)$ is the original Hofstadter butterfly spectrum. Introduction of nonzero β deforms the spectrum in such a way that, for instance, the spectral weight at the band center (van Hove singularity at $\epsilon=0$) for $\alpha=0$ is smeared, and a quasigap develops there with increasing β. The bottommost panel $(\beta=\frac{1}{2})$ is identical to the topmost one except that the spectrum is shifted by $\frac{1}{2}$ along the horizontal (α) axis. That this should be so can be readily understood by recalling the following: At $\beta=\frac{1}{2}$, two adjacent cells enclose $+\frac{1}{2}$ and $-\frac{1}{2}$ flux, respectively. Addition of a uniform flux $\alpha=\frac{1}{2}$ to the system changes them to 1 and 0, which is equivalent to the $(\alpha=0,\beta=0)$ configuration. The same relation (shift by half-period) holds between the spectra for $\beta=\frac{3}{8}$ [panel (d)] and for $\beta=\frac{1}{8}$ [panel (b)]. At $\beta=\frac{1}{4}$ [panel (c)], the periodicity in α becomes half the original one. In other words, the states at $\alpha=$integer and at $\alpha=$half-integer become equivalent for $\beta=\frac{1}{4}$. Again, this can be easily understood by recalling that the flux configuration of two adjacent cells is $(+\frac{3}{4},+\frac{1}{4})$ at $(\beta=\frac{1}{4},\alpha=\frac{1}{2})$, which is equivalent to $(-\frac{1}{4},+\frac{1}{4})$, and hence to $(+\frac{1}{4},-\frac{1}{4})$ at $(\beta=\frac{1}{4},\alpha=0)$.

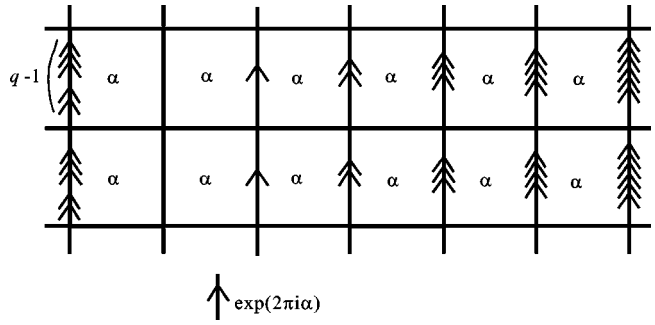

FIG. 1. Tight-binding square lattice with assignment of the Peierls phase factor to each bond, for a uniform external magnetic flux $\alpha=p/q$.

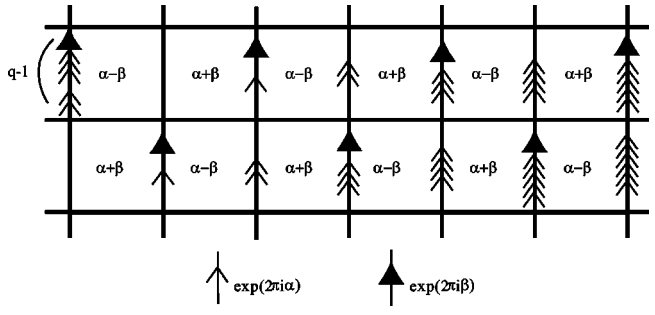

FIG. 2. Square lattice subjected to a spatially varying magnetic field in a checkerboard pattern (β) and a uniform field (α). The assignment of the Peierls phase factor is indicated by the arrows.

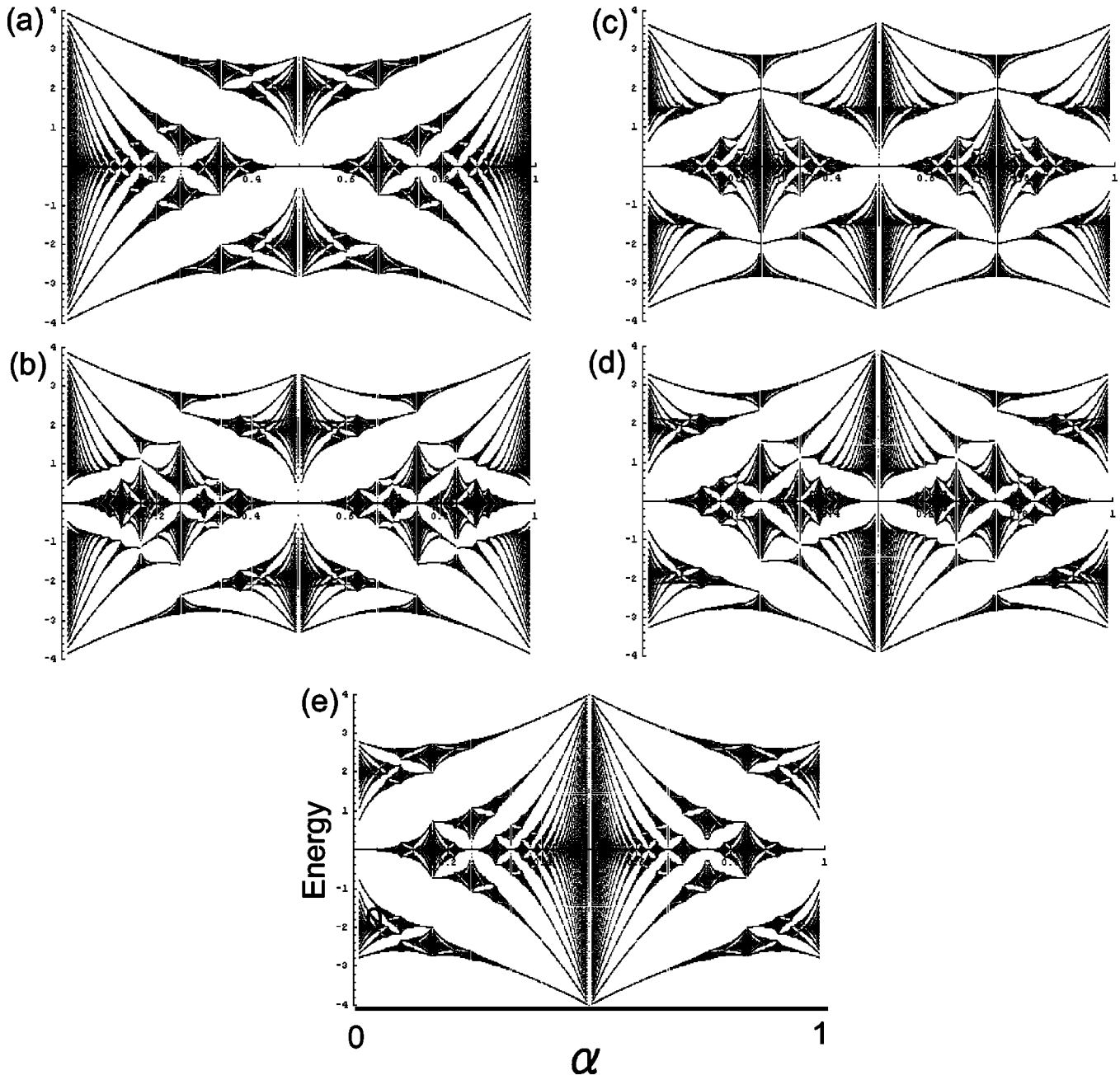

FIG. 3. Hofstadter spectra for a square lattice subjected to a checkerboard field (β) and a uniform field (α). Five panels shows spectra for different amplitudes of the checkerboard field: (a) $\beta=0$, (b) $\beta=\frac{1}{8}$, (c) $\beta=\frac{1}{4}$, (d) $\beta=\frac{3}{8}$, and (e) $\beta=\frac{1}{2}$, respectively.

C. Stripe magnetic field

We next consider the case of a stripe pattern of field modulation, as shown in Fig. 4. Here, β' denotes the flux per plaquette, which alternates in sign for every other column. The assignment of the Peierls phase factor for this flux pattern is shown in the figure. The magnetic unit cell for $\alpha=p/q$ is $(2qa,a)$, i.e., the system is invariant under translation by $(2qa,0)$ or $(0,a)$. The relevant Schrödinger equation reads

$$\varepsilon\psi_{n,m} = t\psi_{n-1,m} + t\psi_{n+1,m} + te^{-2\pi i n\alpha}e^{2\pi i\beta'}\psi_{n,m-1} + te^{2\pi i n\alpha}e^{2\pi i\beta'}\psi_{n,m+1}\ (n \text{ odd}), \quad (6)$$

$$\varepsilon\psi_{n,m} = t\psi_{n-1,m} + t\psi_{n+1,m} + te^{-2\pi i n\alpha}\psi_{n,m-1} + te^{2\pi i n\alpha}\psi_{n,m+1}\ (n \text{ even}).$$

The spectra obtained by diagonalization of the corresponding $2q\times 2q$ matrix are shown in Fig. 5. Only the spectra for $\beta'=\frac{1}{8}$ and $\frac{1}{4}$ are shown, since the spectra for $\beta'=0$ and $\beta'=\frac{1}{2}$ are identical to those for $\beta=0$ and $\beta=\frac{1}{2}$ in Fig. 3, and the spectrum for $\beta'=\frac{3}{8}$ is none other than that for $\beta'=\frac{1}{8}$ shifted by $\frac{1}{2}$ along the horizontal (α) axis. We can immediately note the differences between the spectra for a stripe field and those for a checkerboard field. Introduction of nonzero β' (stripe field) causes lifting of degeneracy

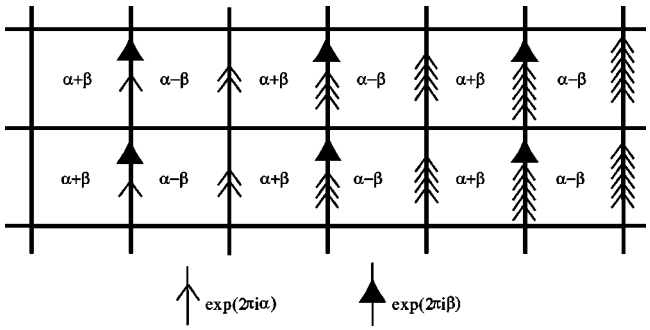

FIG. 4. Square lattice subjected to a spatially varying magnetic field in a stripe pattern (β') and a uniform field (α). The assignment of the Peierls phase factor is indicated by the arrows.

at $\epsilon=0$ for $\alpha=\frac{1}{2}$, while the splitting occurs at integer α for the checkerboard field, as seen earlier. It is evident that the spectra for stripe fields are considerably "darker" (more bands and fewer gaps) as compared with those for checkerboard fields. This is in line with a general trend that the Hofstadter spectrum becomes "darker" as one introduces rectangular anisotropy in the square lattice.[9]

D. Comparison with a honeycomb lattice

Although it is a kind of excursion to a side road, it is interesting to compare the spectra for the checkerboard field shown in Fig. 3 with that for a honeycomb lattice under a uniform magnetic field. Let us consider a square lattice shown in Fig. 6(a), in which the transfer integral for every other vertical bond t' (dotted lines) can take a different value from that for the rest of the bonds t (solid lines).

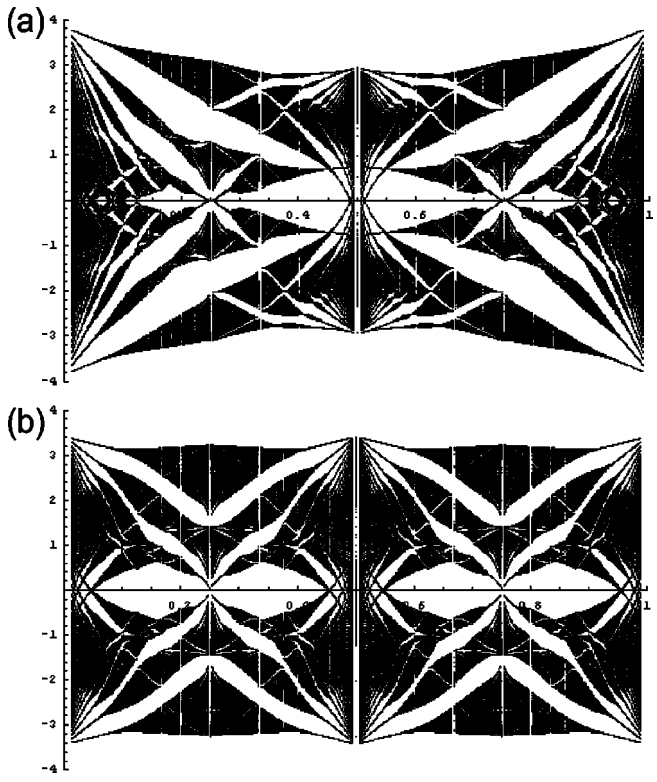

FIG. 5. Hofstadter spectra for different values of β', the strength of the stripe pattern field. (a) $\beta'=\frac{1}{8}$ and (b) $\beta'=\frac{1}{4}$. The spectra for $\beta'=0$ and $\beta'=\frac{1}{2}$ are identical with Figs. 3(a) and 3(e), respectively. The spectrum for $\beta'=\frac{3}{8}$ is the same as the one for $\beta'=\frac{1}{8}$ except it is shifted by $\frac{1}{2}$ along the horizontal (α) axis.

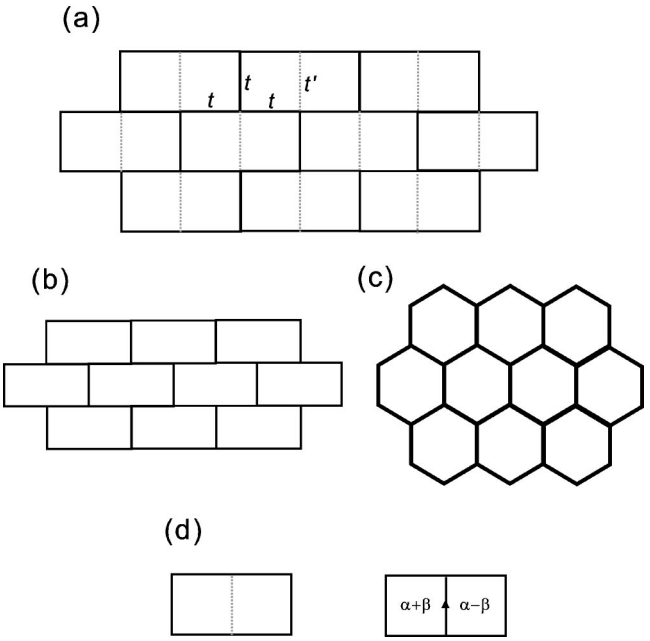

FIG. 6. (a) A square lattice with different transfer integrals t' and t. When $t'=0$ [panel (b)], it is topologically equivalent to a honeycomb lattice [panel (c)]. Panel (d) shows unit "brick" of this lattice and the one for a square lattice under checkerboard field (Fig. 2).

The relevant Schrödinger equation reads

$$\varepsilon\psi_{n,m}=t\psi_{n-1,m}+t\psi_{n+1,m}+te^{-2\pi in\alpha}\psi_{n,m-1}+t'e^{2\pi in\alpha}\psi_{n,m+1}. \tag{7}$$

Setting $t'=t$ reduces the system to a simple square lattice. On the other hand, setting $t'=0$ [Fig. 6(b)] makes it topologically equivalent to a honeycomb lattice [Fig. 6(c)]. Therefore, by changing the parameter t' from t to 0, the system evolves continuously from a square to a honeycomb lattice.

Figure 7 shows calculated spectra for (a) $t'=0.5t$ and (b) $t'=0$ (honeycomb lattice). It is seen that they exhibit a resemblance in overall shape with the spectra for $\beta=\frac{1}{8}$ and $\frac{1}{4}$ for the checkerboard field [panels (b) and (c) of Fig. 3]. The resemblance actually runs over the whole range of the two models, i.e., between the checkerboard field [Eq. (6)] with β changing from 0 to $\frac{1}{2}$ and the square-to-honeycomb evolution [Eq. (7)] with t' changing from t through 0 to $-t$. The spectra at both ends are indeed identical: $(\beta=0)\Leftrightarrow(t'=t)$ and $(\beta=1/2)\Leftrightarrow(t'=-t)$.

In retrospect, this resemblance is something one should have anticipated, because in both cases the structural unit is a rectangle consisting of two adjacent unit squares, as shown in Fig. 6(d). Both Fig. 2 and Fig. 6(a) are then constructed by bricklaying these unit rectangles in the

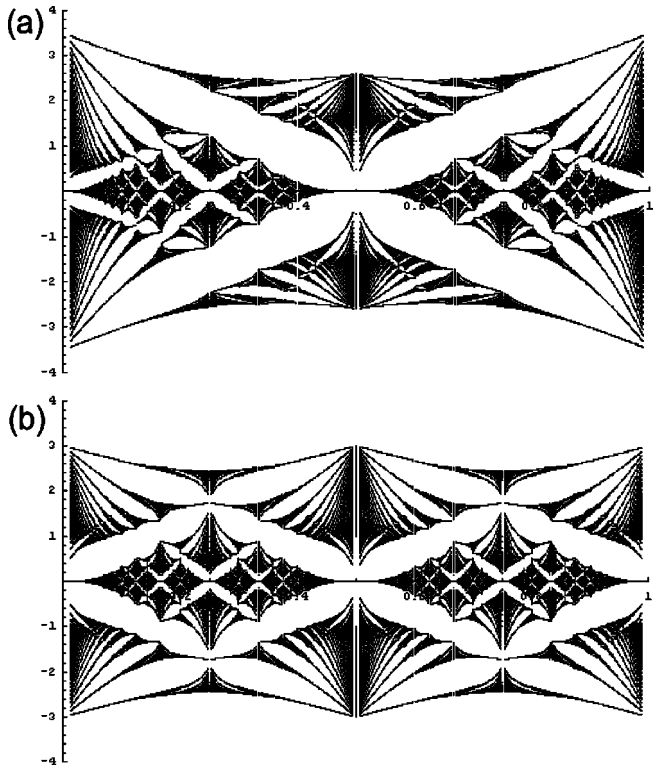

FIG. 7. Spectra for the model defined in Fig. 6. The panels (a) and (b) are for $t'=0.5t$ and 0 (honeycomb lattice), respectively. The spectra for $t'=t$ and $t'=-t$ are the same as the panels (a) and (e) of Fig. 3, respectively.

pattern shown in Fig. 6(b). It is also interesting to note that the spectra shown in Fig. 3 resemble those obtained for a lattice fermion model in the context of two-dimensional d-wave superconductivity.[23]

E. Relation to superconducting networks

The transition temperature of a superconducting wire network under a uniform magnetic field H is related with the eigenvalue $\varepsilon_{\max}$ corresponding to the upper edge of the energy spectrum for the tight-binding model by the following relation:[11–13]

$$\frac{\Delta T_c(H)}{T_{c0}} = \frac{\xi^2(0)}{a^2} \arccos^2\left(\frac{\varepsilon_{\max}}{z}\right). \tag{8}$$

Here, z is the number of nearest-neighbor nodes. Typically, the relative change in the transition temperature is small ($|\Delta T_c| \ll T_{c0}$), and ΔT_c is linearly related with $\varepsilon_{\max}$.

Figure 8 shows the evolution of the lower edge of the Hofstadter spectra as a function of the amplitude (a) β of the checkerboard field and (b) β' of the stripe field. (Since the upper and the lower edge are identical, we show the latter for the sake of ease of visual comparison with the experimental data to be shown later.) The curve on the front-left face (β or $\beta'=0$) represents the lower edge of the original Hofstadter butterfly spectrum. In Fig. 9, the same set of data are presented as a gray-scale plot. A notable difference between the checkerboard and stripe field case is manifest upon comparison of the curves on the front-right face (α=integer). The curve in Fig. 8(a) has a cusp at $\beta=\frac{1}{2}$, while that in Fig. 8(b) is rounded at $\beta'=\frac{1}{2}$. Correspondingly, the latter rises more steeply near the origin than the former. These features are to be compared with the experimental results in the next section. An interesting feature of the energy landscape shown in Fig. 8(a) is that the energy at $\alpha=\frac{1}{4}$ and $\frac{3}{4}$ is constant ($=-2\sqrt{2}$) irrespective of the value of β, which can be seen more clearly in the contour plot of Fig. 9(a).

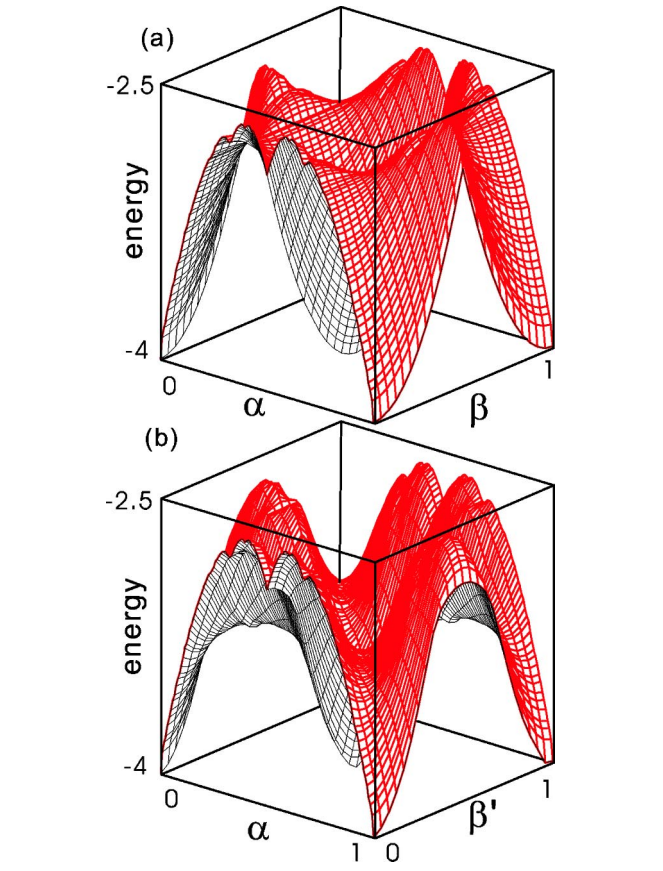

FIG. 8. Stereo plot of the minimum energy as a function of α and β (or β'). Namely, these figures show evolution of the bottom edge of the Hofstadter spectrum with the amplitude of the spatially varying magnetic field of (a) the checkerboard pattern and (b) the stripe pattern.

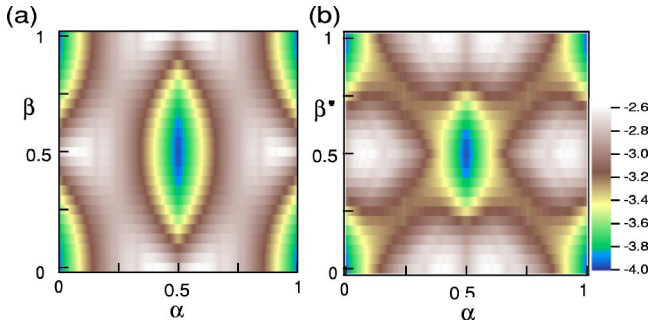

FIG. 9. Contour plot of the same set of data as Fig. 8.

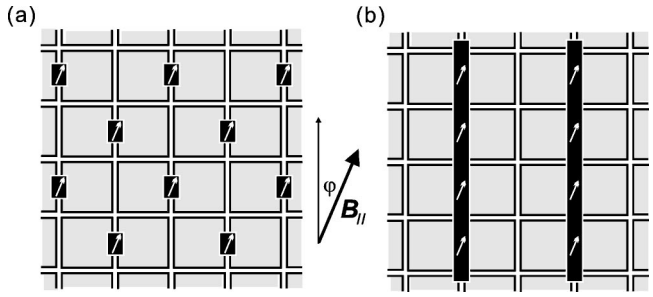

FIG. 10. Structure of the samples. (a) Sample *A* for the checkerboard field. (b) Sample *B* for the stripe field. The external field parallel to the network plane controls the magnetization of the ferromagnetic array. The amplitude of the spatially modulated magnetic field can be changed by the azimuthal angle φ of the parallel field.

III. EXPERIMENT WITH SUPERCONDUCTING WIRE NETWORKS

A. Experimental method

The samples used in the present study were fabricated on silicon substrates by the following steps.

(i) Electrode pads were first formed by electron beam lithography and gold evaporation.

(ii) The network pattern (square lattice) was defined by electron beam lithography and the niobium wire network was formed by ion-beam sputtering deposition and the liftoff process.

(iii) A protecting layer of germanium was deposited on top of the wire network, so as to prevent oxidation of niobium and to keep it from direct contact with the ferromagnetic material to be deposited next.

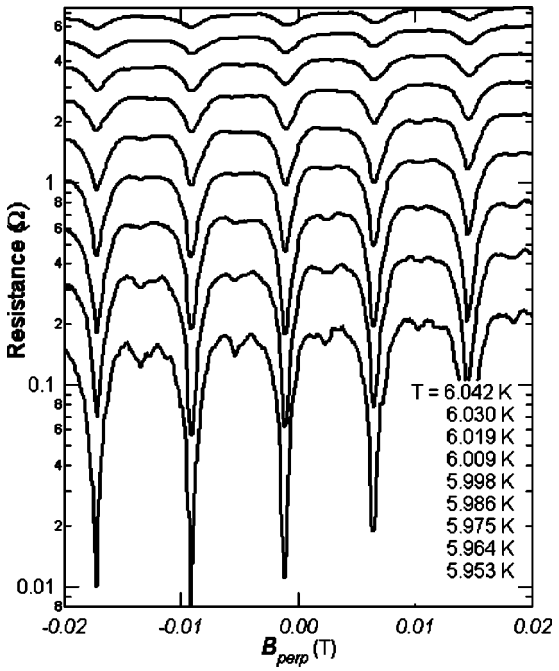

FIG. 11. Magnetoresistance traces at different temperatures for sample *A*. These data were taken at $\varphi=0$, i.e., $\beta=0$.

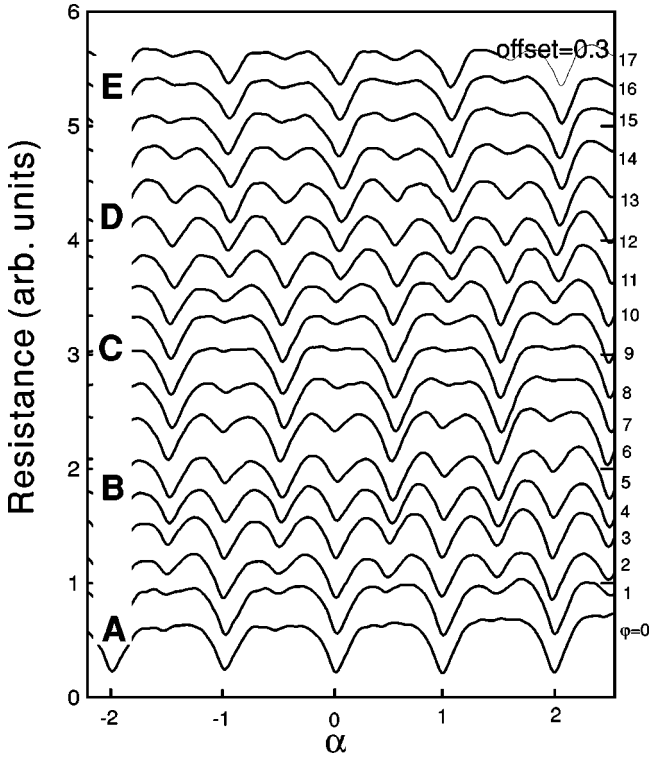

FIG. 12. Evolution of the Little-Parks oscillation for sample *A* with the value of β (checkerboard field). The traces are vertically offset for clarity.

(iv) An array of mesoscopic ferromagnets (cobalt or nickel) was placed on top by electron beam lithography, ion-beam sputter deposition, and liftoff.

The crucial point in the fabrication was to achieve good positional and angular registration between the superconducting network and the overlaid ferromagnet array.

Two samples (*A* and *B*) were intensively studied. These samples represent the checkerboard field case (sample *A*) and the stripe field case (sample *B*), respectively. The superconductor part of the sample consisted of a square network of 100×100 unit cells, made of niobium wire 150 nm wide and 40 nm thick. The lattice period was 500 nm for sample *A* and 750 nm for sample *B*. For sample *A*, 150×200 nm^2 rectangular dots of 80-nm-thick cobalt were placed on top of the center of every other bond wires in the *y* direction, as shown in Fig. 10(a). For sample B, 250-nm-wide strips of 60-nm-thick nickel were placed on top of every other lines in the *y* direction as shown in Fig. 10(b).

Measurements of the superconducting properties were conducted by use of a cross-coil superconducting magnet system, consisting of a 6 T Helmholtz coil and a 1 T solenoid. The horizontal field was used to fix the magnetization of the ferromagnetic array and thereby control the strength of the spatially varying field (parameter β or β'). The vertical field supplied the uniform field (parameter α) for the network. The four-terminal resistance of the network was measured by a standard ac lock-in technique. Cryogenic control was achieved by a variable temperature insert Dewar

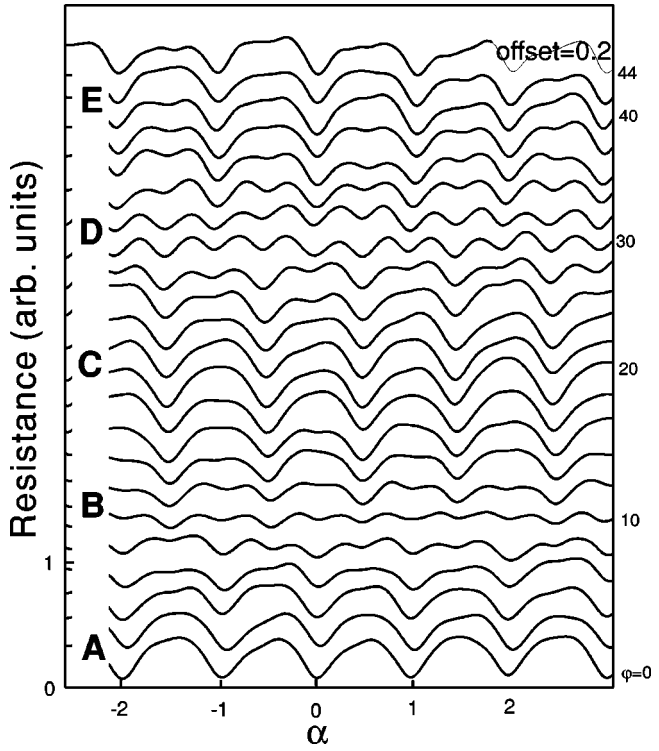

FIG. 13. Evolution of the Little-Parks oscillation for sample *B* with the value of β' (stripe field). The traces are vertically offset for clarity.

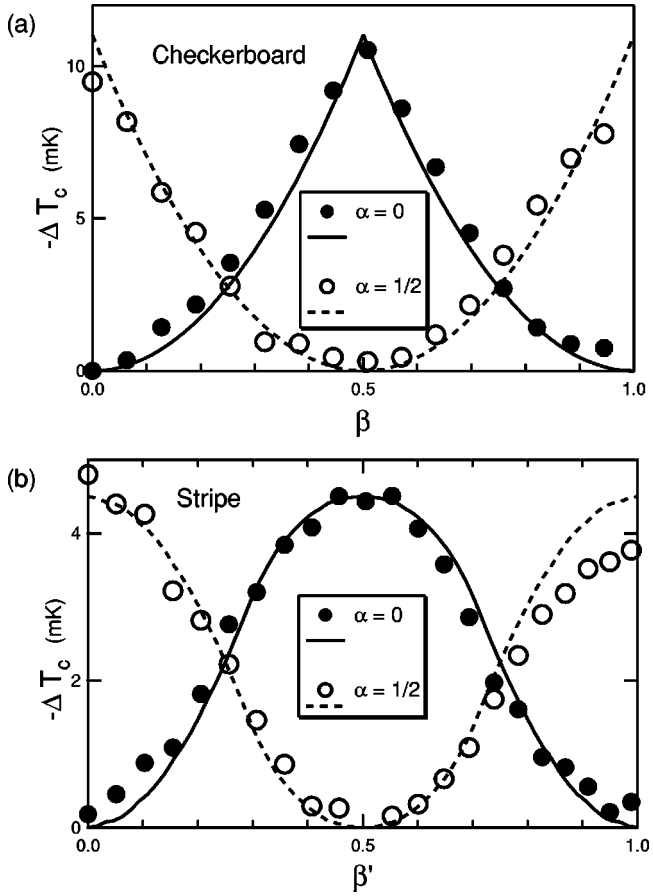

FIG. 14. Comparison of ΔT_c with the edge of the Hofstadter spectra for (a) checkerboard and (b) stripe field. The symbols represent $-\Delta T_c$ obtained from the resistance change as a function of β or β'. The curves represent the bottom edge of the corresponding Hofstadter spectra scaled to fit with the experimental data. The solid symbols and the solid curve correspond to $\alpha=0$. The open symbols and the dashed curve correspond to $\alpha=\frac{1}{2}$.

and a feedback circuit for heater power. Use of a sample holder with rotating stage enabled us to precisely align the orientation of the network sample with respect to the magnetic field.

The plane of the wire network was adjusted so as to make it parallel to the horizontal magnetic field. The horizontal magnetic field was typically set at 1 T, which was strong enough to fully saturate the magnetization of the ferromagnet. The value of β for the checkerboard field (or β' for stripe field) was varied by changing the azimuthal angle φ of the horizontal field. As is clear from the configuration shown in Fig. 10, when $\varphi=0$ the total flux due to the stray field from the mesoscopic magnets adds up to zero for each plaquette (provided that the lithographical symmetry is perfect), so this corresponds to $\beta=0$. As the horizontal field is rotated from $\varphi=0$, the flux piercing each plaquette grows in magnitude, and the sign alternates between adjacent cells. The value of β could thus be controlled in a contiunuous manner (roughly proportional to φ for small φ). A typical set of measurements consisted of sweeping the vertical magnetic field for different settings of φ.

B. Results and discussion

Figure 11 shows a series of magnetoresistance traces for sample *A* under $\varphi=0$ at different temperatures below T_c. Little-Parks oscillations with period 7.7 mT, which agrees well with the unit-cell area $\sim 0.25\ \mu m^2$, are clearly seen with additional dips at half-integers. The small shift of zero magnetic field is due to residual misalignment between the horizontal magnetic field and the film plane. The fine structures at rational values of α other than $\frac{1}{2}$ (and weaker features at $\frac{1}{3}$ and $\frac{2}{3}$) were not clearly observed in this sample. This is probably attributable to lithographical imperfection, especially nonperfect registry between the superconducting wire network and the mesoscopic magnet array, which tends to smear the higher-order structures.

Then the temperature was fixed at a point where the sample resistance was about $0.01R_n$, and a series of magnetoresistance traces were taken by sweeping the vertical field for different settings of φ. Figure 12 shows the traces thus obtained. Here, successive traces correspond to increments of φ by 1 degree, and they are vertically offset for clarity. The horizontal axis is converted to α, with a proper correction for the above-mentioned zero-field shift.

The trace marked *A* corresponds to $\beta=0$. With increments of φ, the dips at half-integers deepen and those at integers become shallow, until they become equal for the trace *B*. Here, the period of oscillation becomes half the original one. This corresponds to $\beta=\frac{1}{4}$. With a further increase

of φ, the dips at half-integer and integer α's change over in depth. The trace *C*, which corresponds to $\beta=\frac{1}{2}$, is shifted by a half-period from the original one (trace *A*). The evolution with β thus goes on and completes one cycle at the trace *E*.

Figure 13 shows a similar set of traces for sample *B*, representing the stripe field case.[24] Although the overall evolution of the trace with β' is similar to Fig. 12, there are two distinct features to be noted. First, comparing the traces *B* in the two figures, the relative amplitude of oscillation at the point of half-periodicity for sample *B* $\left(\beta'=\frac{1}{4}\right)$ is much smaller than the corresponding one for sample *A* $\left(\beta=\frac{1}{4}\right)$. Secondly, although difficult to see directly from Figs. 12 and 13, there is a substantial difference in the way the depth of integer dips (and that of the half-integer dips) evolves with β or β', between the two cases. This is more clearly seen in Fig. 14, which shows the shift in the transition temperature with β (or β') for the two cases. The values of ΔT_c were obtained from the experimentally measured changes in resistance by converting them with use of the resistive transition curve $R(T)$. The amplitude ΔT_c is consistent with Eq. (8) with $\xi(0)\sim 30$ nm. The difference in ΔT_c by a factor of 2 between samples *A* (checkerboard) and *B* (stripe) is chiefly due to the difference in the unit-cell area a^2. The curves in the figure represent the shape of the bottom edge of the corresponding Hofstadter spectra, seen on the front-right facet of the stereo plot in Fig. 8. The solid symbols and the solid curve correspond to $\alpha=0$. The open symbols and the dashed curve correspond to $\alpha=\frac{1}{2}$. The agreement between the experimental data and the calculated curves indicates that the present system of a superconducting network with magnetic decoration captures some of the characteristic features of the Hofstadter spectra under the spatially modulated magnetic field discussed in this paper.

IV. CONCLUSION

We have calculated the Hofstadter butterfly spectra for a 2D tight-binding square lattice subjected to a spatially modulated magnetic field. The corresponding experimental situations are realized by fabricating a superconducting wire network decorated with a mesoscopic ferromagnet array. The evolution of Little-Parks oscillation with the amplitude of the modulated magnetic field in these samples exhibits characteristic features of the two different types of modulation, that is, checkerboard and stripe pattern. These results establish the consistency of the calculated Hofstadter spectra with the change in T_c, although there is a fundamental limitation that only the edge of the spectrum can be probed by the superconducting system.

Control of flux distribution in the superconducting network by mesoscopic magnetic decoration may prove to be a useful technique in the development of devices using superconducting flux quanta. It should be of much interest to explore the vortex dynamics in these artificial potential landscapes. More generally, the mesoscopic ferromagnet/superconductor hybrid system may provide a wider arena for the exploration of vortex physics and possible device applications.

ACKNOWLEDGMENTS

We thank Professor D. Yoshioka, Professor H. Aoki, Professor H. Fukuyama, Professor S. Maekawa, Professor F. Nori, and Dr. M. Koshino for helpful conversations. This work has been supported by a Grant-in-Aid for COE Research "Quantum Dot and Its Application" (No. 12CE2004), and by a Grant-in-Aid for Scientific Research (No. 13304025), from the Ministry of Education, Culture, Sports, Science and Technology (MEXT), Japan.

*Electronic address: iye@issp.u-tokyo.ac.jp

[1] D.R. Hofstadter, Phys. Rev. B **14**, 2239 (1976).
[2] G.H. Wannier, Phys. Status Solidi B **88**, 757 (1978).
[3] F.H. Claro and G.H. Wannier, Phys. Rev. B **19**, 6068 (1979).
[4] Y. Hatsugai and M. Kohmoto, Phys. Rev. B **42**, 8282 (1990).
[5] Ch. Kreft and R. Seiler, J. Math. Phys. **37**, 5207 (1996).
[6] D.J. Thouless, M. Kohmoto, M.P. Nightingale, and M. den Nijs, Phys. Rev. Lett. **49**, 405 (1982).
[7] A.H. MacDonald, Phys. Rev. B **28**, 6713 (1983).
[8] P. Lederer, D. Poilblanc, and T.M. Rice, Phys. Rev. Lett. **63**, 1519 (1989).
[9] Y. Hasegawa, Y. Hatsugai, M. Kohmoto, and G. Montambaux, Phys. Rev. B **41**, 9174 (1990).
[10] C. Albrecht, J.H. Smet, K. von Klitzing, D. Weiss, V. Umansky, and H. Schweizer, Phys. Rev. Lett. **86**, 147 (2001).
[11] B. Pannetier, J. Chaussy, R. Rammal, and J.C. Villegier, Phys. Rev. Lett. **53**, 1845 (1985); see also B. Pennetier, in *Quantum Coherence in Mesoscopic Systems*, edited by B. Kramer, NATO Advanced Study Institute Series Vol. 254 (Plenum Press, New York, 1991), p. 457.
[12] S. Alexander, Phys. Rev. B **27**, 1541 (1983).
[13] R. Rammal, T.C. Lubensky, and G. Toulouse, Phys. Rev. B **27**, 2820 (1983).
[14] M.J. Higgins, Y. Xiao, S. Bhattacharya, P.M. Chaikin, S. Sethuraman, R. Bojko, and D. Spencer, Phys. Rev. B **61**, R894 (2000).
[15] C.C. Abilio, P. Butaud, Th. Fournier, B. Pannetier, J. Vidal, S. Tedesco, and B. Dalzotto, Phys. Rev. Lett. **83**, 5102 (1999).
[16] M.A. Itzler, A.M. Behrooz, C.W. Wilks, R. Bojko, and P.M. Chaikin, Phys. Rev. B **42**, 8319 (1990).
[17] M.A. Itzler, R. Bojko, and P.M. Chaikin, Phys. Rev. B **47**, 14 165 (1993).
[18] B. Doucot, W. Wang, J. Chaussy, B. Pannetier, R. Rammal, A. Vareille, and D. Henry, Phys. Rev. Lett. **57**, 1235 (1986).
[19] S. Ito, M. Ando, S. Katsumoto, and Y. Iye, J. Phys. Soc. Jpn. **68**, 3158 (1999).
[20] M. Ando, S. Ito, S. Katsumoto, and Y. Iye, J. Phys. Soc. Jpn. **68**, 3462 (1999).
[21] Y. Nozaki, Y. Otani, K. Runge, H. Miyajima, B. Pannetier, J.P. Nozieres, and G. Fillion, J. Appl. Phys. **79**, 8571 (1996).
[22] G.-Y. Oh, Phys. Rev. B **62**, 4567 (2000).

[23] Y. Morita and Y. Hatsugai, Phys. Rev. Lett. **86**, 151 (2001).

[24] The reason why the range of φ for Fig. 13 is wider than for Fig. 12 is simply due to the difference in the magnetic decoration. First, the ferromagnetic material for sample *B* was nickel in contrast to cobalt for sample *A*. Secondly, the distance between the ferromagnet array and the superconducting network was about five times larger for sample *B* than sample *A*. These two factors made the value of φ required for the same amplitude of magnetic field modulation much larger for sample *B* than for sample *A*.